https://doi.org/10.5194/acp-2020-957
Preprint. Discussion started: 12 October 2020

Atmospheric Chemistry and Physics Discussions

Future changes in Beijing haze events under different anthropogenic aerosol emission scenarios

Lixia Zhang[1,2], Laura J. Wilcox[3], Nick J. Dunstone[4], David J. Paynter[5], Shuai Hu[1,6], Massimo Bollasina[7], Donghuan Li[9], Jonathan K. P. Shonk[3,8], and Liwei Zou[1]

1 LASG, Institute of Atmospheric Physics, Chinese Academy of Sciences, Beijing, China

2 Collaborative Innovation Center on Forecast and Evaluation of Meteorological Disasters, Nanjing University of Information Science & Technology, Nanjing, 210044, China

3 National Centre for Atmospheric Science, Department of Meteorology, University of Reading, UK

4 Met Office Hadley Centre, FitzRoy Road, Exeter EX1 3PB, UK

5 NOAA/Geophysical Fluid Dynamics Laboratory, Princeton, New Jersey

6 University of Chinese Academy of Sciences, Beijing 100049, China

7 School of Geosciences, Grant Institute, University of Edinburgh, Edinburgh, UK

8 Now at: MetOffice@Reading, Department of Meteorology, University of Reading, UK

9 Key Laboratory of Water Cycle and Related Land Surface Processes, Institute of Geographic Sciences and Natural Resources Research, Chinese Academy of Sciences

Submitted to Atmospheric Chemistry and Physics

Revised on 10th Sep, 2020

Corresponding author: Dr. Lixia Zhang

LASG, Institute of Atmospheric Physics, Chinese Academy of Sciences, Beijing 100029, China

Phone: 86-10-8299-5456 Email: lixiazhang@mail.iap.ac.cn

https://doi.org/10.5194/acp-2020-957
Preprint. Discussion started: 12 October 2020

Atmospheric Chemistry and Physics
Discussions

Abstract: Air pollution is a major issue in China and one of the largest threats to public health. We investigated future changes in atmospheric circulation patterns associated with haze events in the Beijing region, and the severity of haze events during these circulation conditions, from 2016 to 2049 under two different aerosol scenarios: a maximum technically feasible aerosol reduction (MTFR) and a current legislation aerosol scenario (CLE). In both cases greenhouse gas emissions follow the Representative Concentration Pathway (RCP) 4.5. Under RCP4.5 with CLE aerosol the frequency of circulation patterns associated with haze events increases due to a weakening of the East Asian winter monsoon via increased sea level pressure over the North Pacific. The rapid reduction in anthropogenic aerosol and precursor emissions in MTFR further increases the frequency of circulation patterns associated with haze events, due to further increases of the sea level pressure over the North Pacific and a reduction in the intensity of the Siberian high. Even with the aggressive aerosol reductions in MTFR periods of poor visibility, represented by above normal aerosol optical depth (AOD), still occur in conjunction with atmospheric circulation patterns currently associated with haze in the current climate. However, the intensity of poor visibility decreases in MTFR, so that haze events are less dangerous in this scenario by 2050 compared to CLE, and relative to the current baseline. This study reveals the competing effects of aerosol emission reductions on future haze events through their direct contribution to haze and their influence on the atmospheric circulation patterns. A compound consideration of these two impacts should be taken in future policy making.

Key Words: air-pollution, anthropogenic aerosol, atmospheric circulation, haze events

https://doi.org/10.5194/acp-2020-957
Preprint. Discussion started: 12 October 2020

Atmospheric Chemistry and Physics Discussions

1. Introduction

The increases in aerosol and precursor emissions in China due to the rapid economic development and urbanization in recent decades have caused more frequent and severe haze events (Wang et al., 2013; Chen and Wang, 2015). Beijing and the surrounding area is the most polluted region in China (Niu et al., 2010; Ding and Liu, 2014; An et al., 2015; Chen and Wang, 2015). Air pollution has become one of the major issues in China, and the greatest threat to public health. Since the implementation of the "Atmospheric Pollution Prevention and Control Action Plan" in 2013, aerosol emissions have dramatically decreased, with sulphur dioxide (SO_2) reduced by 59% in 2017 compared to 2013 (Zheng et al., 2018). However, haze events have still occurred regularly in recent years, as, in addition to being influenced by aerosol emissions, meteorological conditions, including limited scavenging, dispersion and ventilation, have been found to play important roles in the variation of air-quality in northern China (An et al., 2015; Chen and Wang, 2015; Pei et al., 2018; Cai et al., 2017). Such events are typically associated with the occurrence of large-scale atmospheric circulation patterns favoring the accumulation of pollutants (Yan et al., 2018). Locally, a strong temperature inversion in the lower troposphere, weak surface winds, and subsiding air in the planetary boundary layer are favorable for the development and persistence of haze events (Wu et al., 2017; Feng et al., 2018). As anthropogenic aerosol has the potential to induce changes in the atmospheric circulation, in addition to making a direct contribution to the chemical composition of haze, it is crucial to understand how

https://doi.org/10.5194/acp-2020-957
Preprint. Discussion started: 12 October 2020

changes in aerosol emissions might contribute to the frequency and intensity of haze events in future.

On interannual time scales, the East Asian winter monsoon (EAWM) is significantly negatively correlated with aerosol concentrations in Beijing, due to the associated high frequency of extreme anomalous southerly episodes in North China, a weakened East Asian trough in the mid-troposphere and a northward shift of the East Asian jet stream in the upper troposphere (Jeong and Part, 2017; Li et al., 2016; Pei et al., 2018). The cold air process over Beijing is favorable for pollutant dispersion and transport outside because of the accompanied large near-surface wind speed and deep mixing layer. A low occurrence of cold air processes in the recent winters of 2013, 2014 and 2017 has resulted in severe pollution (He et al., 2018). In past decades, the weakening of the EAWM was found to contribute to the increased frequency of haze events over North China (Chen and Wang, 2015; An et al., 2015). Arctic sea ice extent also has been linked to increased stability over eastern China and has been shown to explain 45%~67% of the interannual to interdecadal variability of winter haze days over eastern China (Wang et al., 2015). Overall, around half of the variability in the frequency of haze events in Beijing is controlled by meteorological conditions, while both meteorological conditions and aerosol emissions contribute to the intensity (Pei et al., 2020).

Anthropogenic forcing, estimated by using large ensemble runs with and without anthropogenic forcings, has increased the probability of the atmospheric patterns

https://doi.org/10.5194/acp-2020-957
Preprint. Discussion started: 12 October 2020

conducive to severe haze in Beijing by weakening the EAWM (Li et al., 2018). Projections based on Coupled Model Intercomparison Project Phase 5 (CMIP5) models showed that weather conditions conducive to haze events in Beijing will increase with global warming due to an increased occurrence of stagnation days in response to both accelerated Arctic ice melting (Cai et al., 2017; Liu et al., 2019) and a continued weakening of EAWM (Hori et al., 2006; Pei et al., 2018; Liu et al., 2019). If there is no change in aerosol emission in future, increased stagnation days and decreased light precipitation days associated with global warming would also cause an increase in air pollution days in eastern China (Chen et al., 2019). Regional climate model simulations under the RCP4.5 scenario showed that the air environment carrying capacity, a combined metric measuring the capacity of the atmosphere to transport and dilute pollutants, tends to decrease in the 21st century across China (Han et al., 2017). However, there is large uncertainty in future aerosol emission pathways, with uncertainty around the sign of the change in global emission rate, as well as the magnitude of the change (Scannell et al., 2019). Furthermore, changes in aerosol emission may influence haze events through their influence on the large-scale atmospheric circulation, in addition to their role in haze composition.

The interplay between the role of aerosol as a constituent of haze, and as a potential driver of changes in the circulation patterns conducive to haze, have yet to be explored. If the rapid reductions in aerosol and precursor emissions currently underway in China continue in future, understanding the balance between the different influences of

https://doi.org/10.5194/acp-2020-957
Preprint. Discussion started: 12 October 2020

anthropogenic aerosol on haze events is a key question. Typically, anthropogenic aerosol (AA) and greenhouse gases (GHGs) both vary in future simulations (e.g. those following the RCPs or Shared Socioeconomic Pathways), which can make their relative contributions difficult to determine. In this work, we examine future scenarios with the same GHGs emission pathway but different aerosol pathways in order to separate these two contributions to changes in Beijing haze events. We address three questions: 1) Do the atmospheric conditions conducive to haze events change in future? 2) Do aerosol reductions contribute to this change? 3) If the frequency of atmospheric conditions conducive to haze events increases in future, do local aerosol reductions act to moderate the severity of the haze events?

The remainder of the paper is organized as follows: we briefly introduce the experiment design and methods in Section 2, and show the model performance in simulating atmospheric circulation patterns conducive to Beijing haze events in Section 3. Projected Beijing haze events under two different aerosol emissions and the underlying mechanism of projected circulation changes will be given in Section 4. We will finally provide the summary and discussion in Section 5.

2. Experiments and methods

2.1 Experiment design

We use simulations with the Met Office Unified Model (Global Coupled configuration 2) HadGEM3-GC2 (Williams et al., 2015) and the NOAA Geophysical

https://doi.org/10.5194/acp-2020-957
Preprint. Discussion started: 12 October 2020

Fluid Dynamics Laboratory (GFDL) Climate Model version 3 (GFDL-CM3, Donner et al. 2011; Griffies et al. 2011). GFDL-CM3 has a horizontal resolution of ~200 km in the atmosphere and 1º in the ocean. HadGEM3-GC2 is run with a horizontal resolution of N216 (~60 km) in the atmosphere, and ¼º in the ocean. Both models include a representation of aerosol-cloud interactions (Ming et al., 2006; Bellouin et al., 2007). We employed two models to check the robustness of the results.

Three sets of experiments were carried out with each model (Table S1): a historical experiment (His) from 1965 to 2015 and two experiments for the future (2016-2049). In the historical experiment, greenhouse gases and anthropogenic aerosol and precursor emissions are taken from CMIP5 (Lamarque et al., 2010, Taylor et al., 2012). The future experiments have common GHG emissions following the RCP4.5 scenario, but different aerosol emission pathways. The aerosol pathways are the current legislation emissions (CLE) and the maximum technically feasible reduction (MTFR) taken from the ECLIPSE V5a global emission dataset (Amann et al., 2015, https://iiasa.ac.at/web/home/research/researchPrograms/air/ECLIPSEv5a.html). In CLE, anthropogenic aerosol emissions are assumed to evolve following the current legislation, resulting in a moderate global increase by 2050. In contrast, MTFR assumes a full implementation of the most advanced technology presently available to reduce aerosol emissions by 2030, which results in their rapid global decrease over this period. The regional changes in AA for His, CLE and MTFR can be found in Scannell et al. (2019) and Luo et al. (2020).

We use 1980-2004 as a baseline, 2016-2049 as the future period, and display anomalies between the two. The difference between the future and baseline winter (December to February) mean SO_2 emissions over China is shown in Fig.S1 for CLE and MTFR. Compared with His, CLE shows a dramatic increase in SO_2 over Asia, with peak values over India and eastern China (Fig.S1a). MTFR has similar changes over Europe to CLE (not shown), negligible changes over India, and a dipole over China, with a weak increase to the north and a decrease to the south (Fig.S1b). Thus, a dramatic decrease in SO_2 in MTFR relative to CLE is seen over the whole Asian continent, particularly over the Beijing region (30-45°N, 100-120°E; Fig. S1c).

Data from the Japanese 55-year Reanalysis (JRA55; Kobayashi et al., 2015) dataset for the period 1958-2013 are used in this study to evaluate the model representations of the present-day climate.

2.2 Haze Weather Index

We focus on haze events during the winter (December-February) around Beijing where Chinese haze events are most frequent and severe (Niu et al., 2010; Chen and Wang, 2015). Several large-scale metrics have been proposed to identify haze events (Ding et al., 2017; Feng et al., 2019; Pei et al., 2018). In general, Beijing haze events are accompanied by weaker surface winds, high atmospheric stability, and fewer cold air outbreaks. To capture all of these features in a single metric, we use the haze weather index (HWI) proposed by Cai et al. (2017) as it has also been shown to have a strong relationship with PM2.5 concentrations in Beijing.

https://doi.org/10.5194/acp-2020-957
Preprint. Discussion started: 12 October 2020

The HWI comprises three constituent terms representing the vertical temperature gradient in the troposphere (ΔT), the 850-hPa meridional wind (V850), and the north—south shear in the 500-hPa zonal wind (U500) (see boxes and lines in Fig.1). ΔT is calculated as the difference between the 850 hPa temperature averaged over (32.5°–45°N, 112.5°–132.5°E) and the 250-hPa temperature averaged over (37.5°–45°N, 122.5°–137.5°E). V850 is the 850hPa meridional wind averaged over the broader Beijing region (30°–47.5°N, 115°–130°E), and U500 is a latitudinal difference between the 500-hPa zonal wind averaged over a region to the north of Beijing (42.5°–52.5° N, 110°–137.5°E) and a region to the south (27.5°–37.5°N, 110°–137.5°E). Each of the three terms is normalized by their standard deviation over the reference period (here 1980-2004). The three variables are added together to create the HWI, which is then normalized again by its standard deviation over the reference period. A positive HWI represents conditions that are unfavorable to air-pollutant dispersion, and days with HWI>0 are regarded as “haze events”. The HWI defined by Cai et al. (2017) made use of daily data. Due to unavailability of model data at daily resolution, we instead used monthly data. The reliability of using HWI calculated from monthly mean variables will be discussed in Section 3.

2.3 East Asian winter monsoon index

The strength of the EAWM index is quantified using the index defined by Wang and Chen (2014). This index takes into account both the east-west and the north-south pressure gradients and is defined as:

https://doi.org/10.5194/acp-2020-957
Preprint. Discussion started: 12 October 2020

$$EAWM=(2*SLP_1-SLP_2-SLP_3)/2$$

where SLP_1, SLP_2 and SLP_3 represent normalized sea level pressure (SLP) averaged over Siberia (40-60°N, 70-120°E), the North Pacific (30-50°N, 140°E-170°W) and the Maritime Continent (20°S-10°N, 110-160°E), respectively (see the boxes in Fig.S2). The three components are converted to anomalies and normalized by their standard deviation over the reference period (here 1980-2004). As the EAWM is directly linked to the occurrence of favorable conditions for haze in Beijing (Pei et al. 2018; Liu et al. 2019; Hori et al. 2006), we therefore use this index as an additional metric (using different variables to the HWI) to assess the potential for changes in future haze events under the CLE and MTFR scenarios, and confirm the robustness of the changes indicated by HWI.

3. Climatic conditions associated with Beijing haze events

The circulation anomalies averaged over the days with daily HWI greater than 1.0 are shown in Fig.1a, c, e. The vertical temperature profile shows warmer air at the lower to mid-levels, centered around 850hPa and cold anomalies aloft 250hPa (Fig.1a). Thus, the atmosphere is stable, unfavorable for the vertical dispersion of pollutants. At the mid-latitude (500hPa), we see northward shifted mid-level westerly jets (Fig.1c). The weakened westerly winds along 30°N is difficult for the horizontal dispersion of pollutants out of Beijing. At the lower-level, the anomalous southerly winds at 850hPa along the East Asian coast lead to a reduction in the prevailing surface cold northerlies in winter (Fig.1e). This reduction favors warmer conditions at lower levels and

https://doi.org/10.5194/acp-2020-957
Preprint. Discussion started: 12 October 2020

increased moisture over Beijing, thus increasing the likelihood of haze formation and maintenance.

The HWI was defined based on daily data. Due to limitations in data availability, we instead used monthly data to calculate HWI. To determine the reliability of this approach, we first examined the relationship between the magnitude of HWI calculated from monthly data (HWI-month) and the number of days with daily HWI (HWI-daily) > 0 in the JRA-55 reanalysis during the period 1958-2013 (Fig. 2). Changes in HWI-month are highly consistent with those in haze events days (r = 0.97). The scatter plots between HWI-monthly and the monthly mean of HWI-daily also demonstrates their high correlation (0.98). When HWI-month is greater than 0, about 50% days in that month are recognized as haze days, and up to 62% days with HWI-daily >0 when HWI-month ≥ 1.0. In this study, we define a 'haze event' as a month where HWI-month ≥ 1, as around 62% of days within this month are likely to be haze days. The circulation anomalies averaged over HWI-month ≥ 1 (Fig. 1b, d, f) and HWI-daily > 0 (Fig. 1a, c, e) are also consistent with each other, except that the anomalies for HWI-month≥1 are weaker, as would be expected. The spatial and temporal consistency of HWI anomalies calculated from monthly and daily data confirms the suitability of our use of monthly data to explore changes in the frequency of Beijing haze events associated circulation. In the following sections, we will use HWI in short for HWI-month.

Both HadGEM3-GC2 and GFDL-CM3 well simulate the key spatial features of the large-scale atmospheric circulation in winter, when compared to JRA-55 for 1980-

https://doi.org/10.5194/acp-2020-957
Preprint. Discussion started: 12 October 2020

Atmospheric Chemistry and Physics Discussions
Open Access
EGU

2004 (Fig.S3). Key features include the westerly jet along 30°N, the East Asian trough, and northerly winds along the East Asian coast, which are caused by the zonal thermal contrast and subsequent pressure gradient between the North Pacific and the Eurasian continent. The models can also reliably capture the vertical temperature difference, the weaker East Asian trough and the anomalous 500-hPa southerly winds associated with haze events (Fig.S4). The good performance of HadGEM3-GC2 and GFDL-CM3 in simulating the climate mean state demonstrates their suitability to explore the changes in circulation patterns associated with haze events under different AA emission scenarios.

4. Changes in Beijing haze events under two AA emission scenarios

4.1 Changes in the frequency of circulation patterns conducive to haze events

The time series of winter HWI in the historical simulation and two different future scenarios from each member of HadGEM3-GC2 and GFDL-CM3 are shown in Fig.3a-b. There is large interannual variability in the index, and thus no significant trend in HWI either in His, CLE or MTFR. However, the two models both show an increase in the mean HWI with no consistent change in the standard deviation. The mean HWI in His (1980-2014), CLE (2016-2049) and MTFR (2016-2049) is 0, 0.40, and 0.65 in HadGEM3-GC2. In GFDL-CM3 it is 0, 0.40, and 0.53. A slight increase in the standard deviation of HWI is simulated by HadGEM3-GC2 from His (1.0) and CLE (1.0) to MTFR (1.06), while no change is seen in GFDL-CM3.

https://doi.org/10.5194/acp-2020-957
Preprint. Discussion started: 12 October 2020

The occurrence of positive HWI in CLE and MTFR increases relative to His in both models, as shown in Fig.3c-d. We find a shift of the HWI distribution toward the right, indicating an increased occurrence of weather conditions conducive to Beijing haze events in CLE and MTFR, particularly in MTFR. We employed the two-sample Kolmogorov-Smirnov test to determine if the HWI distributions from each period and experiment are significantly different (Chakravarti et al. 1967). In both models, the HWI distributions in His and CLE are significantly different at the 1% level. The distributions of HWI in CLE and MTFR are also significantly different at the 1% level in HadGEM3-GC2, but insignificant in GFDL-CM3, although GFDL-CM3 shows a much larger frequency of $1<HWI<2$ in MTFR compared to CLE. The changes in the frequency of the different HWI bins used in Fig.3 are shown in Table 1. The frequency of $HWI \geq 1$ for His, CLE and MTFR is ~16% (15.7%), 28.6% (27.3%), and 35.7% (34.6%) in HadGEM3-GC2 (GFDL-CM3), respectively. If AA emissions follow the CLE scenario, the frequency of $HWI \geq 1$ will increase by 12.6% and 11.6% in HadGEM3-GC2 and GFDL-CM3 respectively. The rapid reduction in AA emissions in MTFR contributes to an extra 7% increase in HWI relative to CLE in both models.

The shift in the HWI distributions shown in Fig. 3c-d is also associated with increase in atmospheric circulation patterns currently associated with the most severe haze events. Very extreme events ($HWI \geq 3$) in HadGEM3-GC2 account for only 0.3% of the total historical events. This almost doubles in CLE, and increases by a factor of 5 in MTFR. This kind of event never happened in the current baseline of GFDL-CM3,

https://doi.org/10.5194/acp-2020-957
Preprint. Discussion started: 12 October 2020

Atmospheric Chemistry and Physics Discussions

but accounts for about 0.3% of events in MTFR. This change indicates that both greenhouse gas increases and aerosol reductions may increase the frequency of occurrence of the atmospheric circulation pattern currently associated with severe haze events over the Beijing region.

An examination of the future changes in each component of the HWI is shown in Fig.4. The shift of HWI towards more positive values from His to CLE, with a larger shift in MTFR relative to His, is found in all three components. This shift is mainly caused by the increase in the mean values of ΔT, U500 and V850. In both models, the distributions of all the component terms of the His are statistically different between His and CLE and MTFR (at the 5% level). As for HWI, the distributions of the three component terms are significantly different between CLE and MTFR in HadGEM3-GC2, but not GFDL-CM3. For HadGEM3-GC2 (GFDL-CM3), the frequencies of $\Delta T \geq 1$, $U500 \geq 1$ and $V850 \geq 1$ have increased from 14.0%, 17.0%, and 7.2% (16.7%, 18.0%, and 17.8%) in His to 29.3%, 26.8%, and 16.0% (30.2%, 25.1%, and 22.2%) in CLE, and to 37.2%, 36.3%, and 22.7% (25.8%, 32.7%, and 23.1%) in MTFR. The changes of the three components of HWI demonstrate the atmospheric conditions favoring haze events all become more likely with global warming, and that future AA reductions may further increase their likelihood.

4.2 Possible mechanism for atmospheric circulation changes

Section 4.1 showed that the projected change of mean state of the large-scale atmospheric circulation in the future will increase the frequency of circulation patterns

https://doi.org/10.5194/acp-2020-957
Preprint. Discussion started: 12 October 2020

Atmospheric Chemistry and Physics Discussions

currently associated with Beijing haze events. Rapid reductions in AA emissions could cause a further increase. To investigate the mechanism underlying these circulation changes, we present the spatial patterns of the changes in the vertical temperature profile, and 850-hPa and 500-hPa winds in Figs.5-7. The lower- and mid-troposphere displays an incremental warming from His to MTFR compared to the upper levels in both models. The peak warming is at 700 hPa and over 120°-130°E. Conversely, both models simulate an upper-tropospheric cooling at 250 hPa in CLE compared to His, albeit of smaller magnitude than the warming below (Fig.S5 a-b, e-f). However, the 250 hPa temperature changes differ in the two models (Fig.5b, d and Fig.S5 c-d, g-h). Thus, the increase in tropospheric stability in MTFR relative to CLE is mainly driven by low-level warming.

Following the CLE aerosol pathway, both HadGEM3-GC2 and GFDL-CM3 project an anomalous 850-hPa cyclonic circulation over the northwestern Pacific (0-20°N, 120-180°E) relative to His, and an anticyclonic anomaly to its north (20-50°N, 120-180°E) (Fig.6a-b). This pattern bears some resemblance to the anomalous circulation associated with a positive phase of the Arctic Oscillation, which may be due to melting Arctic sea ice (Shindell et al. 1999; Fyfe et al. 1999; Chen et al. 2017; Wang et al. 2017). The southerly wind anomalies over eastern China, on the western flank of the anomalous anticyclone, act to weaken the East Asian winter monsoon and reduce its low-level winds, making conditions favorable for air-pollutant transport from south to north and air-pollutant accumulation more likely. With the addition of rapid AA

https://doi.org/10.5194/acp-2020-957
Preprint. Discussion started: 12 October 2020

Atmospheric Chemistry and Physics Discussions

reductions following MTFR, the 850-hPa circulation anomalies are reinforced further (Fig6.c-d), especially in HadGEM3-GC2, which simulates much stronger southerly wind anomalies along the East Asian coast. GFDL-CM3 shows similar anomalies over the North Pacific in CLE vs. His and MTFR vs. CLE, but distinct responses over China (Fig.6d), which likely explains why GFDL-CM3 doesn't simulate the further shift in HWI seen in HadGEM3-GC2 between CLE and MTFR (Fig.4e, f and Table S2). A northeasterly anomaly is seen over southeast China in GFDL-CM3 in both CLE relative to His and MTFR relative to CLE. However, the onshore flow over Beijing seen in CLE relative to His, which is likely to be a key contributor to an increase in haze weather events, is not enhanced further by the rapid aerosol reductions in MTFR (Fig. 6d).

At 500 hPa, a northward shift of the westerly jet stream is projected in CLE relative to the current baseline, with significant positive zonal wind anomalies along 50°N and negative anomalies along 30°N in both models (Fig.7a-b). This shift is consistent with the increase in the meridional temperature gradient over the North Pacific (Fig.S5). Thus, the East Asian winter trough is weakened, bringing less cold and dry air to the Beijing area, and favoring the formation and maintenance of haze events. The reductions in AA emissions in MTFR relative to CLE significantly strengthen the above-mentioned circulation anomalies at 500 hPa in both models (Fig 7c,d), and further increase the frequency of positive U500 differences in the regions used to calculate the HWI, as seen in Fig.c-d and Table S2. The changes in 500-hPa zonal winds are consistent between the two models, demonstrating the robustness of the results.

https://doi.org/10.5194/acp-2020-957
Preprint. Discussion started: 12 October 2020

The changes in the three components of HWI in CLE relative to His indicate a weakened EAWM with increased GHGs, with reductions in AA emissions further amplifying this effect and increasing the frequency of large-scale circulation conditions conducive to Beijing haze events. To explore how the EAWM circulation responds to reductions in AA emissions, we show surface temperature and sea level pressure changes in MTFR relative to CLE (Fig. 8). Reduced AA emissions generally amplify the impact of greenhouse gases, with more warming over the Arctic, the Eurasian continent and Northwestern Pacific. Thus, the Aleutian low is further weakened in MTFR. In addition, more warming over the Eurasian continent and Northwestern Pacific leads to a SLP decrease over Siberia and the northwestern Pacific, respectively. The main difference between the two models is found from the SLP changes over the Eurasian continent in the mid-latitudes, where large negative SLP anomalies are presented in HadGEM3-GC2 while there are no changes in GFDL-CM3. This may lead to the less westward shift of the North Pacific anomalous anticyclonic circulation in GFDL-CM3 in Fig.6d.

Histograms of EAWM, using the Wang and Chen (2014) index, and its components in His, CLE and MTFR are shown in Fig.9. The EAWM weakens in CLE compared to His (Fig.9a-b), mainly due to increased SLP over the North Pacific (SLP_2, Fig.9e-f), with no systematic changes in SLP over Siberia (SLP_1) and the Maritime continent (SLP_3) (Fig.9a-b, h-g). The rapid AA reductions in MTFR cause the SLP over Siberia to decrease consistently in both models alongside an increase in SLP_1. This

https://doi.org/10.5194/acp-2020-957
Preprint. Discussion started: 12 October 2020

further weakens the east-west contrast, leading to a weaker EAWM in MTFR relative to CLE, consistent with the differences between CLE and His and between MTFR and CLE seen in the HWI. The response of SLP over the Maritime Continent (SLP_3) to AA reductions differs between the two models, indicating large uncertainty in the SLP_3 changes. Thus, the AA forcing reduction predominantly weakens the EAWM through reducing the zonal thermal contrast.

4.3 Changes in haze intensity associated with favoring circulation

Occurrence of a haze event requires stagnant atmospheric conditions, and a pollution source. Although future aerosol reductions may cause further increases in the frequency of atmospheric circulation patterns currently linked with haze events, such events may be less severe in the absence of large aerosol emissions. In this section, we will examine the projected changes in the intensity of Beijing haze events using the aerosol optical depth (AOD) at 550nm as a metric for aerosol-induced poor visibility. The simulated baseline winter mean AOD in the Beijing area is around 0.1 (Fig.10a, c). HadGEM3-GC2 and GFDL-CM3 both simulate elevated AOD around Beijing when circulation conditions are favorable (HWI≥1) (Fig.10 b, d): 1.4 and 1.3 times of the baseline climate mean in HadGEM3-GC2 and GFDL-CM3 respectively. Aerosol and precursor emission increases under CLE (Fig. S1) result in a significant increase in climate winter mean AOD around Beijing (reaching 1.2 times in HadGEM3-GC2 and 1.05 times in GFDL-CM3), while climate mean AOD in MTFR decreases to 0.93 of the baseline climate mean around Beijing in the two models due to aerosol emissions

https://doi.org/10.5194/acp-2020-957
Preprint. Discussion started: 12 October 2020

reduction (Fig.S6).

To check whether poor air quality events still occur even with reduced future aerosol emissions, we show the projected AOD with HWI≥1 as a fraction of the baseline winter mean in Fig.11. In CLE, when HWI≥1 AOD is elevated compared to the baseline climatology (Fig. 11), to 1.6 times of the baseline winter mean in HadGEM3-GC2 and 1.1 times that in GFDL-CM3. It is consistent with the increase in aerosol loadings and climate mean AOD in CLE (Fig.S1a and Fig.S6a-b). However, in MTFR, when HWI≥1 AOD is also higher than the baseline climatology, albeit with a decrease in climate mean AOD in MTFR (Fig.S6c-d). So, even with the aggressive aerosol reductions in MTFR, periods of poor visibility still occur in conjunction with atmospheric circulation patterns associated with haze in the current climate.

The severity of air quality under the circulation patterns favoring haze (when HWI≥1) changes differently between CLE and MTFR. Thus, we compared months when HWI≥1 shows the effect of aerosol emission changes on haze intensity under the same circulation patterns (Fig. 12). For HWI≥1, AOD over Beijing is comparable in CLE to His in HadGEM3-GC2, but slightly reduced in GFDL-CM3, despite the increase in aerosol emissions. This reduction in GFDL-CM3 may be a reflection of the model's bias. In JRA-55 when HWI≥1 there are southerly anomalies over southern China. However, in the baseline in GFDL-CM3 there is an anomalous cyclonic circulation, which may act to reduce pollutant accumulation in Beijing (Fig.S4). As shown in Fig. 6, this anomaly is strengthened in both CLE and MTFR. When HWI≥1

https://doi.org/10.5194/acp-2020-957
Preprint. Discussion started: 12 October 2020

in MTFR, both models show a significant reduction in AOD compared to baseline events when HWI≥1. This demonstrates that the air quality is similar under CLE to the baseline condition under the favorable circulation patterns of haze, but it is much improved under MTFR (Fig.12e-f).

Because AOD dramatically decreases in MTFR relative to His and CLE, the atmospheric circulation patterns with HWI≥1 may not be associated with haze events in this scenario, even though the circulation patterns associated with haze in the baseline become more frequent in the future with aerosol reductions. Then, we further investigated the changes in AOD with different values of HWI in MTFR relative to that in His when HWI≥1 (Fig.S7). In HadGEM3-GC2, when HWI≥2 AOD in Beijing in MTFR is comparable with that in His when HWI≥1. In GFDL-CM3, we see slightly increase in AOD with higher HWI values, but AOD in Beijing with higher HWI is still lower than the current haze events when HWI ≥1. It means that the haze events associated with the circulation patterns currently conducive to haze may become less dangerous with reduced aerosol emissions in future, even though the circulation patterns will be more prevalent. A higher criterion for HWI value may be better to examine the projected changes in haze events if aerosol emissions are reduced.

5 Summary and discussion

During recent decades, with rapid increases in aerosol and precursor emissions in China, air pollution has become one of the greatest threats to public health. Anthropogenic aerosol contributes not only to the chemical composition of haze, but

https://doi.org/10.5194/acp-2020-957
Preprint. Discussion started: 12 October 2020

also has the potential to modulate atmospheric circulation changes. Thus, this paper aims to quantify the incidences of haze events in a future climate and the influence of aerosol mitigation efforts. In this study, we examined the changes in the frequency of atmospheric conditions conducive to Beijing haze events, and the changes in aerosol optical depth (AOD) during these circulation conditions through the mid-21st century under two different anthropogenic aerosol scenarios. We also investigated the mechanism for the changes in the large-scale atmospheric circulation. We found that future greenhouse gases (GHG) increases and anthropogenic aerosol (AA) increases following a current legislation aerosol scenario (CLE) will increase the frequency of atmospheric circulation conditions conducive to Beijing haze events, especially the very extreme circulation patterns. By comparing the scenario with a maximum technically feasible aerosol reduction (MTFR), which has the same GHG increases but rapid aerosol reductions, we show that future aerosol reductions may further amplify the increase in the frequency of such circulation patterns. The frequency of haze weather index (HWI)≥1.0 derived from monthly data increases from ~16% at baseline to ~28% for 2016-2049 under the CLE scenario. Rapid reductions in AA emissions in MTFR contribute to an extra ~7% increase in HWI≥1 in two models: HadGEM3-GC2 and GFDL-CM3. We also find that the frequency of exceptional extreme circulation events with HWI≥3.0 in HadGEM3-GC2 is only 0.3% in His, but is almost doubled in CLE and increases by a factor of 5 in MTFR. These kinds of events never happen in the baseline in GFDL-CM3, but account for 0.3% of events in MTFR.

https://doi.org/10.5194/acp-2020-957
Preprint. Discussion started: 12 October 2020

Atmospheric Chemistry and Physics Discussions

The increase in haze frequency in CLE is mainly due to a weakening of the East Asian winter monsoon, warming of the lower troposphere, and weakening of the East Asian trough, which is likely to be predominantly driven by the GHG increases. Reduced AA forcing in MTFR could further enhance the above circulation anomalies, amplifying the impact of greenhouse gases. Because the AA emission reductions in MTFR relative to CLE mainly occur over continental Asia, the Asian landmass receives more shortwave radiation, leading to a warmer surface temperature there. This leads to a weaker Siberian high, and further contributes to the weakening of the East Asian winter monsoon seen in MTFR.

The analysis of haze intensity based on AOD at 550 nm shows that visibility with HWI$\geq$1.0 is always lower than the His winter mean under both CLE and MTFR. However, in future the haze events associated with HWI$\geq$1.0 are comparable, or less severe, than their baseline equivalents. Under MTFR, there is a marked reduction in the AOD associated with HWI$\geq$1.0 compared to His. This demonstrates that even though the atmospheric circulations that favor haze events will become more frequent as GHG increases and AA decreases, the haze events themselves will become less dangerous if aerosol emissions are reduced.

This paper reveals the competing impacts of AA emission reductions on haze event frequency and intensity. AA reductions cause an increased frequency of atmospheric circulation patterns conducive to haze events, but a reduction in the haze intensity when these circulation patterns do occur. This demonstrates that the local air quality benefits from clean air policies outweigh the dynamical climate impact of aerosol and precursor emission reductions in this case.

Author contribution: L Zhang designed and wrote the manuscript with support from all authors. LJW and MAB helped design the analysis and supervised the work. NJD and DJP ran the simulations. Shuai Hu analyzed the reanalysis data. Donghuan Li and Liwei Zou contributed to the validation of observational metrics.

Acknowledgement: This work was jointly supported by the National Natural Science Foundation of China under grant No. 41675076. LJW, MAB and JKPS were supported by the UK-China Research & Innovation Partnership Fund through the Met Office Climate Science for Service Partnership (CSSP) China as part of the Newton Fund. Liwei Zou is supported by National Natural Science Foundation of China under grant No. 41830966.

Reference:

Amann M., I. Bertok, J. Borken-Kleefeld, J. Cofala, C. Heyes, L. Hoglund-Isaksson, G. Kiesewetter, Z. Klimont, W. Schöpp, N. Vellinga, W. Winiwarter: Adjusted historic emission data, projections, and optimized emission reduction targets for 2030 – A comparison with COM data 2013. Part A: Results for EU-28. TSAP Report #16A, version 1.1. IIASA, Laxenburg, Austria, 2015.

https://doi.org/10.5194/acp-2020-957
Preprint. Discussion started: 12 October 2020

An Z., R. Huang, R. Zhang, X. Tie, G. Li, J. Cao, W. Zhou, Z. Shi, Y. Han, Z. Gu, Y. Ji: Severe haze in northern China: A synergy of anthropogenic emissions and atmospheric processes. Proceedings of the National Academy of Sciences of the United States of America, 116 (18): 8657–8666, https://doi.org/10.1073/pnas.1900125116, 2019.

Cai W J, K. Li, H. Liao, H. Wang, L. Wu: Weather conditions conducive to Beijing severe haze more frequent under climate change, Nat. Clim. Change. 7: 257–62, 2017.

Chakravarti, Laha, and Roy, 1967: Handbook of Methods of Applied Statistics, Volume I, John Wiley and Sons, pp. 392-394.

Chen, H.P., H. J., Wang: Haze Days in North China and the associated atmospheric circulations based on daily visibility data from 1960 to 2012. J. Geophys. Res. Atmos. 120, 5895–5909, https://doi.org/10.1002/2015JD023225, 2015.

Chen H., H. Wang, J. Sun,Y. Xu, Z. Yin: Anthropogenic fine particulate matter pollution will be exacerbated in eastern China due to 21st century GHG warming. Atmospheric Chemistry and Physics, 19, 233–243, https://doi.org/10.5194/acp-19-233-2019, 2019.

Donner , L. J., B. L. Wyman, R. S. Hemler, L. W. Horowitz, Y. Ming et al.: The dynamical core, physical parameterizations, and basic simulation characteristics

https://doi.org/10.5194/acp-2020-957
Preprint. Discussion started: 12 October 2020

of the atmospheric component of the GFDL global coupled model CM3. Journal of Climate, 24, 3484–3519, DOI: 10.1175/2011JCLI3955.1 2011.

Francis JA, Vavrus S J.: Evidence linking Arctic amplification to extreme weather in mid-latitudes. Geophysical Research Letters, 39, 06801, 2012.

Fyfe, J. C., Boer, G. J. and Flato, G. M.: The Arctic and Antarctic oscillations and their projected changes under global warming. Journal of Geophysical Research, 26, 1601–1604, 1999.

Griffies S., M. Winton, L. Donner, et al.: The GFDL CM3 Coupled Climate Model: Characteristics of the Ocean and Sea Ice Simulations. Journal of Climate, 24(13), 3520-3544, 2011.

Han Z., B. Zhou, Y. Xu, J. Wu and Y. Shi: Projected changes in haze pollution potential in China: an ensemble of regional climate model simulations. Atmospheric Chemistry and Physics, 17, 10109–10123. https://doi.org/10.5194/acp-17-10109-2017, 2017.

He J., Gong S., Zhou C. et al.: Analyses of winter circulation types and their impacts on haze pollution in Beijing. Atmospheric Environment, 192, 94–103, 2018.

Hori, M.E. and Ueda, H.: Impact of global warming on the East Asian winter monsoon as revealed by nine coupled atmosphere-ocean GCMs. Geophysical Research Letters, 33(3): L03713, 2006.

https://doi.org/10.5194/acp-2020-957
Preprint. Discussion started: 12 October 2020

Atmospheric Chemistry and Physics Discussions

Kobayashi, S., and Coauthors: The JRA-55 reanalysis: general specifications and basic characteristics. Journal of the Meteorological Society of Japan, 93(1), 5-48,doi:http://doi.org/10.2151/jmsj.2015-001, 2015.

Jeong Jaein I., and Rokjin J. Park: Winter monsoon variability and its impact on aerosol concentrations in East Asia. Environmental Pollution, 221, 285e292, 2017.

Lamarque J, Bond T, Eyring V, et al.: Historical (1850-2000) gridded anthropogenic and biomass burning emissions of reactive gases and aerosols: Methodology and application, Atmospheric Chemistry and Physics, 10: 7017−7039, 2010.

Li, Q., Zhang, R., Wang, Y.: Interannual variation of the wintertime fog-haze days across central and eastern China and its relation with East Asian winter monsoon. International Journal of Climatology. 36, 346e354, 2016.

Li, K., Liao, H., Cai, W., & Yang, Y.: Attribution of anthropogenic influence on atmospheric patterns conducive to recent most severe haze over eastern China. Geophysical Research Letters, 45, 2072–2081. https://doi.org/10.1002/2017GL076570, 2018.

Luo F., L. Wilcox, B. Dong et al.: Projected near-term changes of temperature extremes in Europe and China under different aerosol emissions. Environmental Research Letters, 15,034013, 2020.

Ming Y., V. Ramaswamy, L. J. Donner, and V. T. J. Phillips: A robust parameterization of cloud droplet activation. J. Atmos. Sci., 63, 1348–1356, 2006.

https://doi.org/10.5194/acp-2020-957
Preprint. Discussion started: 12 October 2020

Pei L. and Z. W., Yan: Diminishing clear winter skies in Beijing towards a possible future. Environmental Research Letters, 13,124029, 2018.

Pei L., Z.W, Yan, Z. Sun, S. Miao, Y. Yao: Increasing persistent haze in Beijing: potential impacts of weakening East Asian winter monsoons associated with northwestern Pacific sea surface temperature trends. Atmospheric Chemistry and Physics, 18,3173–83, 2018.

Pei L., Yan Z.W., Chen D., and Miao S.: Climate variability or anthropogenic emissions: which caused Beijing Haze? Environmental Research Letters, 15 034004, 2020.

Scannell, C., and Coauthors: The Influence of Remote Aerosol Forcing from Industrialized Economies on the Future Evolution of East and West African Rainfall. Journal of Climate, 32, 8335–8354, https://doi.org/10.1175/JCLI-D-18-0716.1. 2019.

Screen JA, Simmonds I.: The central role of diminishing sea ice in recent Arctic temperature amplification. Nature, 464, 1334–1337, 2010.

Shindell, D. T., R. L. Miller, G. A. Schmidt, L. Pandolfo: Simulation of recent northern winter climate trends by greenhouse-gas forcing. Nature, 399, 452–455, 1999.

Wang J., W. Qu, C. Li et al.: Spatial distribution of wintertime air pollution in major cities over eastern China: Relationship with the evolution of trough, ridge and synoptic system over East Asia. Atmospheric Research. 212, 186-201, 2018.

https://doi.org/10.5194/acp-2020-957
Preprint. Discussion started: 12 October 2020

Wang, H. J., H. P. Chen, and J. P. Liu: Arctic sea ice decline intensified haze pollution in eastern China, Atmospheric and Oceanic Science Letters, 1–9, 2015.

Wang Y., T. Le, G. Chen, et al.: Reduced European aerosol emissions suppress winter extremes over northern Eurasia. Nature Climate Change,10, 225–230, 2020.

Wilcox L., N. Dunstone, A. Lewinschal, M. Bollasina, A. Ekman, E. Highwood: Mechanisms for a remote response to Asian aerosol emissions in boreal winter. Atmospheric Chemistry and Physics, 19, 9081–95, 2019.

Williams K. D., C. M. Harris, A. Bodas-Salcedo, et al.: The Met office global coupled model 2.0 (GC2) configuration Geoscientific Model Development, 8,1509–24, 2015.

Wu P., Y. Ding, Y. Liu: Atmospheric circulation and dynamic mechanism for persistent haze events in the Beijing–Tianjin–Hebei region. Advances in Atmospheric Sciences, 34, 429–40, doi: 10.1007/s00376-016-6158-z. 2017.

Zhang, L., Liao, H., Li, J.: Impacts of Asian summer monsoon on seasonal and interannual variations of aerosols over eastern China. Journal of Geophysical Research: Atmospheres. 115, 2010.

Zhang, R.H., Li, Q., Zhang, R.N.: Meteorological conditions for the persistent severe fog and haze event over eastern China in January. Science China Earth Sciences, 57, 26–35. https://doi.org/10.1007/s11430-013-4774-3, 2014.

https://doi.org/10.5194/acp-2020-957
Preprint. Discussion started: 12 October 2020

Atmospheric Chemistry and Physics
Discussions

Zheng B., D. Tong, M. Li, et al: Trends in China's anthropogenic emissions since 2010 as the consequence of clean air actions. Atmospheric Chemistry and Physics, 18, 14095–111, 2018.

https://doi.org/10.5194/acp-2020-957
Preprint. Discussion started: 12 October 2020

Atmospheric Chemistry and Physics Discussions

Figure Captions:

Table 1 Frequency (unit: %) of different HWI bins in His, CLE and MTFR

Fig. 1 Composite circulation anomalies from JRA-55 with HWI-daily>0 (left) and HWI-month≥1.0 (right) for 1958-2013. (a)-(b) temperature anomalies (K) along 40°N, (c)-(d) 500hPa winds anomalies (vector, m/s) and 500hPa zonal winds anomalies (shading, m s^{-1}). (e)-(f) 850hPa winds anomalies (vector, m s^{-1}) and 850 hPa meridional winds anomalies (shading, m s^{-1}). The green boxes/lines indicate the location of the boxes/lines used in the calculation of HWI.

Fig.2 Changes in winter HWI from 1958 to 2013 in JRA-55 reanalysis relative to 1958-2013 winter mean. (a) DJF mean monthly-based HWI (HWI-month, black line) and the anomalous days with daily based HWI >0 (HWI-daily, red line, unit: day), (b) scatter plot of HWI-month of the monthly values from December, January and February (y-axis) and HWI-daily averaged in the same month as HWI-month (x-axis). (c) same as (a), but for HWI-month (y-axis) and the ratio of days with HWI-daily>0 (x-axis) in each winter month. HWI-month and HWI-daily are the HWI calculated from monthly data and daily data, respectively.

Fig.3 Changes in HWI in His (grey line), CLE (blue) and MTFR (pink) experiments simulated by (a) HadGEM3-GC2 and (b) GFDL-CM3 for the winters from 1965 to 2049. Histogram plots for HWI frequency (y-axis, %) simulated by (c) HadGEM3-GC2 and (d) GFDL-CM3. The x-axis in (c)-(d) shows different bins

https://doi.org/10.5194/acp-2020-957
Preprint. Discussion started: 12 October 2020

of HWI, and grey, blue and pink bars are for His (1980-2004), CLE (2016-2049) and MTFR (2016-2049), respectively.

Fig.4 Same as Fig.3c-d, but for the histograms of each component of HWI simulated by HadGEM3-GC2 (left) and GFDL-CM3 (right). (a)-(b) ΔT, (c)-(d) U500 and (e)-(f) V850.

Fig.5 The difference in winter mean temperature (K) along 40°N (left) between CLE (2016-2049) and His (1980-2004), and (right) between MTFR (2016-2049) and CLE (2016-2049). The dotted areas are statistically significant at the 10% level.

Fig.6 Spatial distribution for the difference in 850 hPa winds (vector, m s^{-1}) and 850hPa meridional component (shading, m s^{-1}) between (left) CLE (2016-2049) minus historical (1980-2004), and between (right) MTFR (2016-2049) minus CLE (2016-2049). The dotted areas denote the 850hPa meridional winds statistically significant at 90% confidence level.

Fig.7 Same as Fig.6, but for the difference in 500hPa winds (vector, m s^{-1}) and its zonal component (shading, m s^{-1}).

Fig.8 The difference of the climate mean surface temperature (left, K) and sea level pressure (right, hPa) between MTFR and CLE simulated by (a)-(b) HadGEM3-GC2 and (c)-(d) GFDL-CM3.

Fig.9 Same as Fig.4, but for histograms of the East Asian winter monsoon index and its components.

https://doi.org/10.5194/acp-2020-957
Preprint. Discussion started: 12 October 2020

Fig.10 DJF mean (left) AOD at 550 nm in (a) HadGEM3-GC2 and (c) GFDL-CM3 averaged over 1980-2004. Right is same as left, but for the ratio of AOD averaged in the winter months with HWI≥1 relative to winter mean of 1980-2004. Blue and red shadings in (c)-(d) are lower and higher than the climate mean of baseline, respectively.

Fig.11 Same as Fig.10b and d, but for the results projected in CLE and MTFR. The baseline is the winter mean of 1980-2004.

Fig.12 Difference between the ratio of AOD when HWI≥1.0 to His winter mean in CLE and ratio of AOD when HWI≥1.0 to His winter mean in His in (a) HadGEM3-GC2 and (b) GFDL-CM3. (c)-(d) and (e)-(f) are same as (a) and (b), but for the difference between MTFR and His and the difference between MTFR and CLE, respectively. Blue and red shadings indicate projected AOD when HWI≥1.0 is lower and higher than the AOD when HWI≥1.0 in His, respectively.

https://doi.org/10.5194/acp-2020-957
Preprint. Discussion started: 12 October 2020

Atmospheric Chemistry and Physics Discussions
Open Access
EGU

Table 1 Frequency (unit: %) of different HWI bins in His, CLE and MTFR

Model	**Exp**	**HWI bins**						
		0~0.5	**0.5~1**	**1~1.5**	**1.5~2**	**2~2.5**	**2.5~3**	**≥3**
HadGEM3-GC2	His	20.7	16.2	10.0	3.7	1.7	0.3	0.3
	CLE	20.5	17.9	16.2	7.4	3.8	0.7	0.5
	MTFR	18.9	16.7	13.8	10.7	7.2	2.6	1.4
GFDL-CM3	His	18.7	18.7	8.0	5.0	2.7	0.0	0.0
	CLE	19.4	19.7	14.0	7.9	4.4	1.0	0.0
	MTFR	19.4	16.8	14.9	15.2	2.9	1.3	0.3

https://doi.org/10.5194/acp-2020-957
Preprint. Discussion started: 12 October 2020

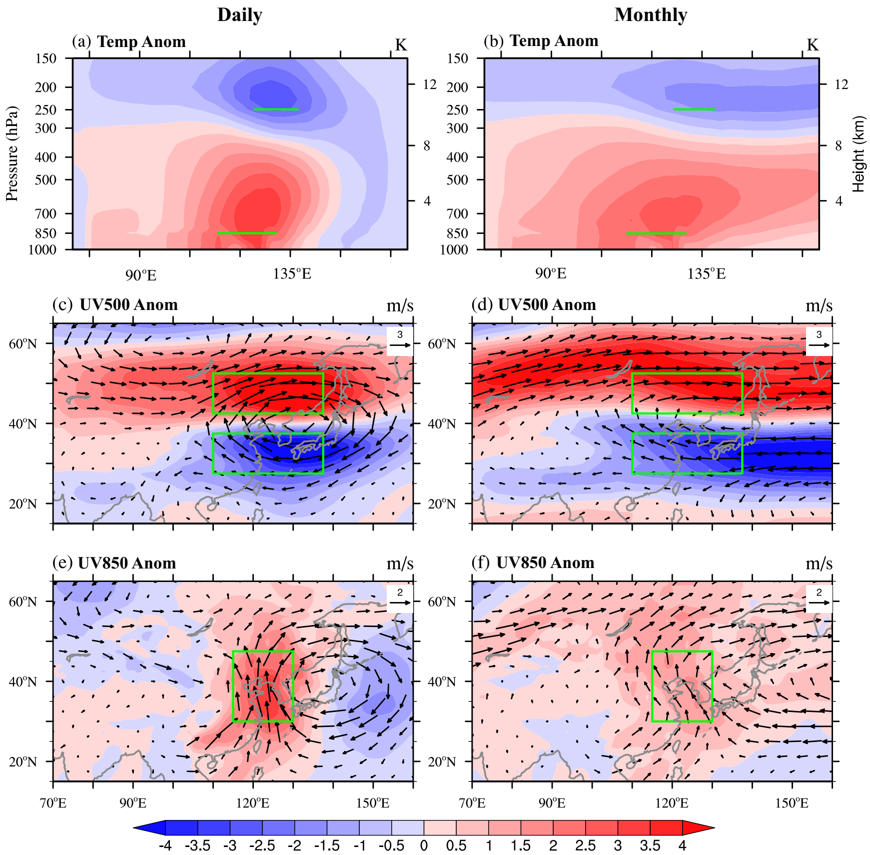

Fig. 1 Composite circulation anomalies from JRA-55 with HWI-daily>0 (left) and HWI-month≥1.0 (right) for 1958-2013. (a)-(b) temperature anomalies (K) along 40°N, (c)-(d) 500hPa winds anomalies (vector, m s^{-1}) and 500hPa zonal winds anomalies (shading, m s^{-1}). (e)-(f) 850hPa winds anomalies (vector, m s^{-1}) and 850 hPa meridional winds anomalies (shading, m s^{-1}). The green boxes/lines indicate the location of the boxes/lines used in the calculation of HWI.

https://doi.org/10.5194/acp-2020-957
Preprint. Discussion started: 12 October 2020

Atmospheric Chemistry and Physics Discussions

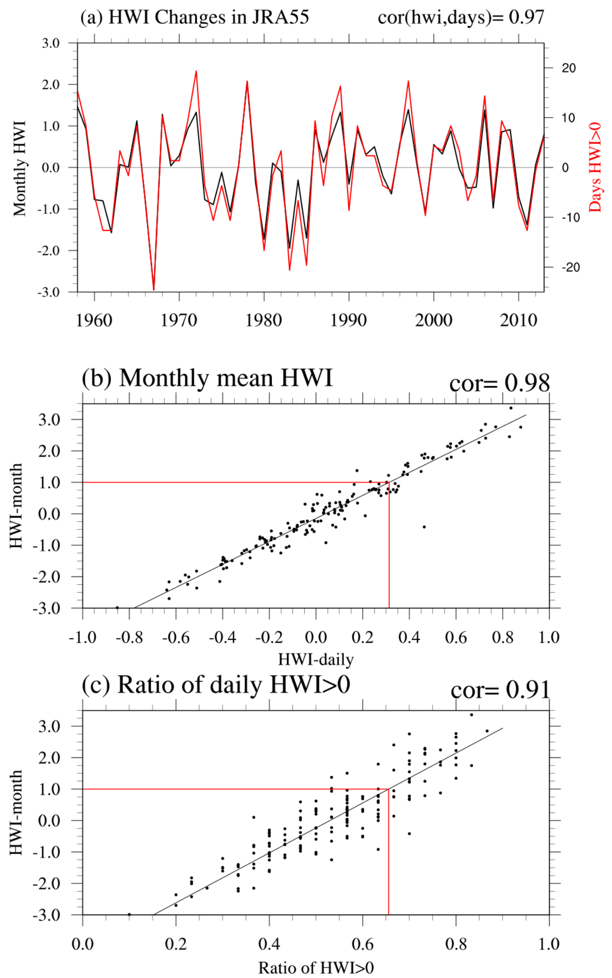

Fig.2 Changes in winter HWI from 1958 to 2013 in JRA-55 reanalysis relative to 1958-2013 winter mean. (a) DJF mean monthly-based HWI (HWI-month, black line) and the anomalous days with daily based HWI >0 (HWI-daily, red line, unit: day), (b) scatter plot of HWI-month of the monthly values from December, January and February (y-axis) and HWI-daily averaged in the same month as HWI-month (x-axis). (c) same as (a), but for HWI-month (y-axis) and the ratio of days with HWI-daily>0 (x-axis) in each winter month. HWI-month and HWI-daily are the HWI calculated from monthly data and daily data, respectively.

https://doi.org/10.5194/acp-2020-957
Preprint. Discussion started: 12 October 2020

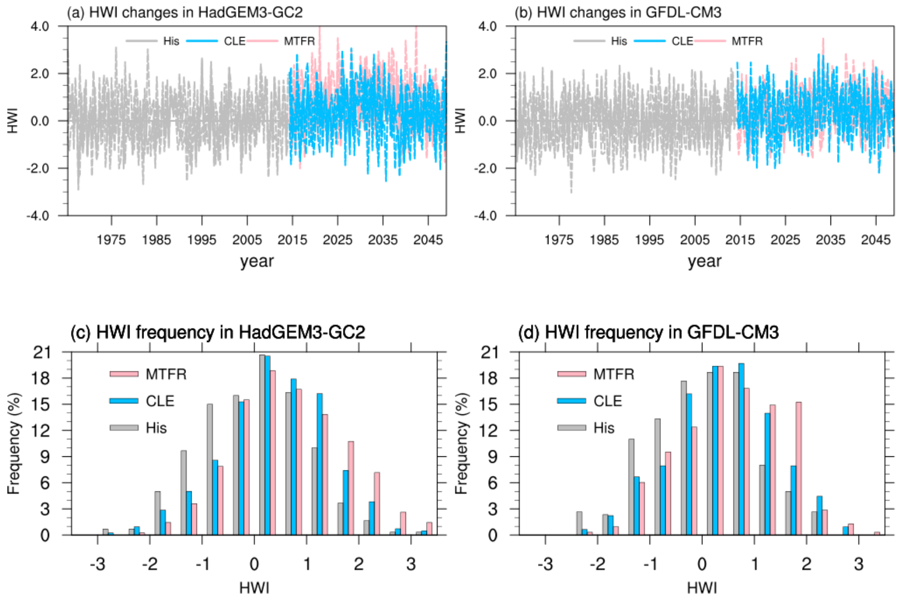

Fig.3 Changes in HWI in His (grey line), CLE (blue) and MTFR (pink) experiments simulated by (a) HadGEM3-GC2 and (b) GFDL-CM3 for the winters from 1965 to 2049. Histogram plots for HWI frequency (y-axis, %)simulated by (c) HadGEM3-GC2 and (d) GFDL-CM3. The x-axis in (c)-(d) shows different bins of HWI, and grey, blue and pink bars are for His (1980-2004), CLE (2016-2049) and MTFR (2016-2049), respectively.

https://doi.org/10.5194/acp-2020-957
Preprint. Discussion started: 12 October 2020

Atmospheric Chemistry and Physics
Discussions

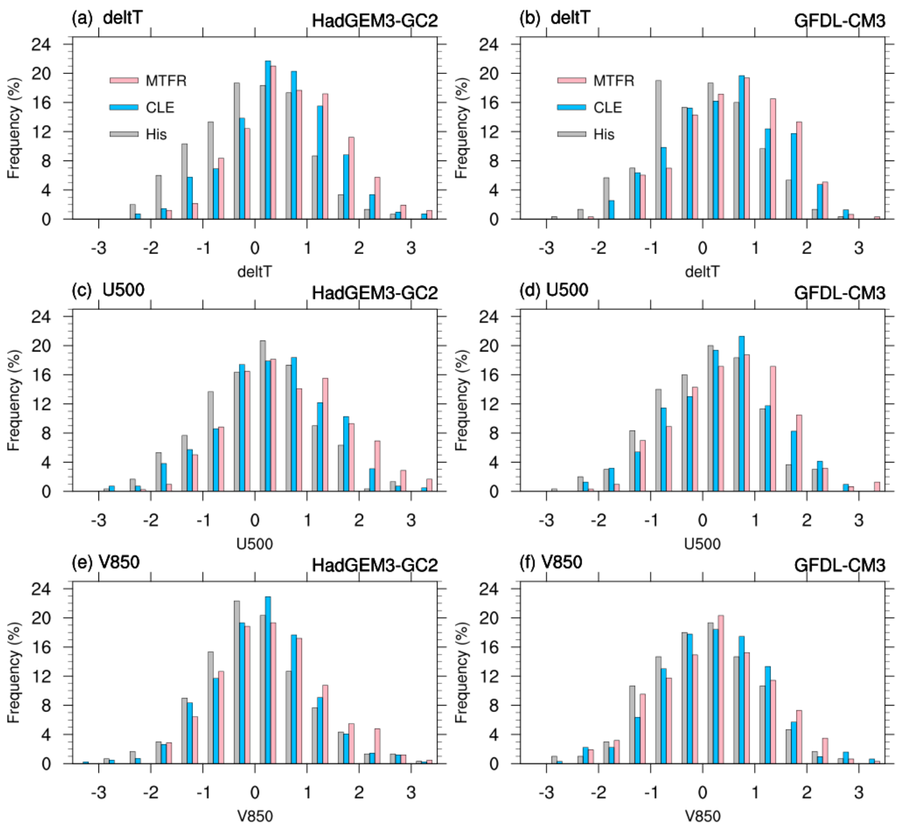

Fig.4 Same as Fig.3c-d, but for the histograms of each component of HWI simulated by HadGEM3-GC2 (left) and GFDL-CM3 (right). (a)-(b) ΔT, (c)-(d) U500 and (e)-(f) V850.

https://doi.org/10.5194/acp-2020-957
Preprint. Discussion started: 12 October 2020

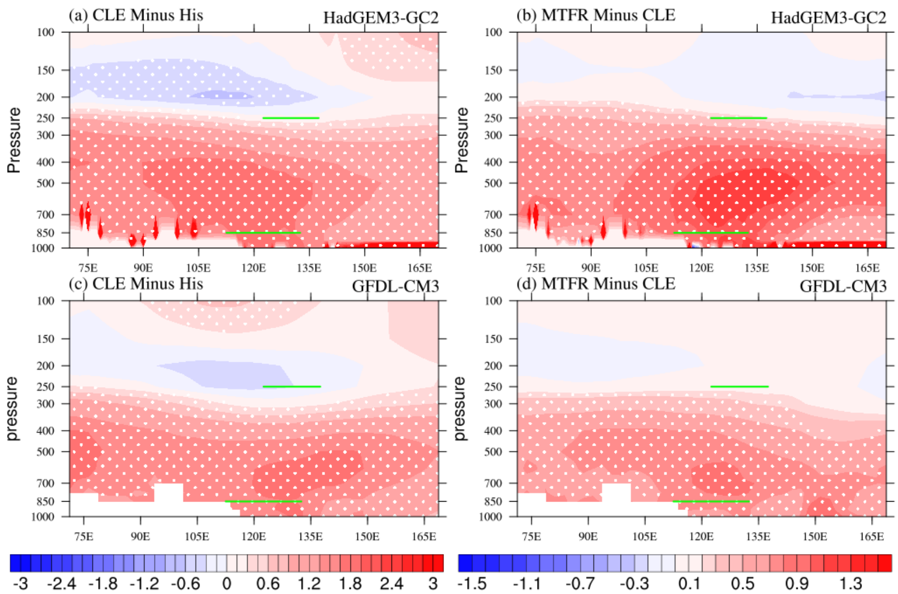

Fig.5 The difference in winter mean temperature (K) along 40°N (left) between CLE (2016-2049) and His (1980-2004), and (right) between MTFR (2016-2049) and CLE (2016-2049). The dotted areas are statistically significant at the 10% level.

https://doi.org/10.5194/acp-2020-957
Preprint. Discussion started: 12 October 2020

Atmospheric Chemistry and Physics
Discussions

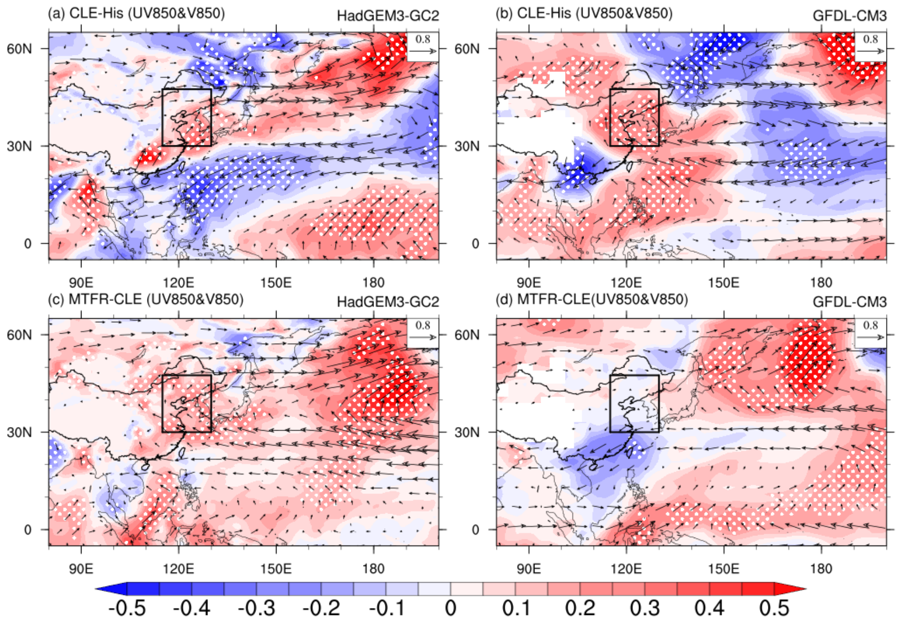

Fig.6 Spatial distribution for the difference in winter mean 850 hPa winds (vector, m s^{-1}) and 850hPa meridional component (shading, m s^{-1}) (left) between CLE (2016-2049) and His (1980-2004), and (right) between MTFR (2016-2049) and CLE (2016-2049). The dotted areas denote the 850hPa meridional winds statistically significant at the 10% level.

https://doi.org/10.5194/acp-2020-957
Preprint. Discussion started: 12 October 2020

Atmospheric Chemistry and Physics Discussions

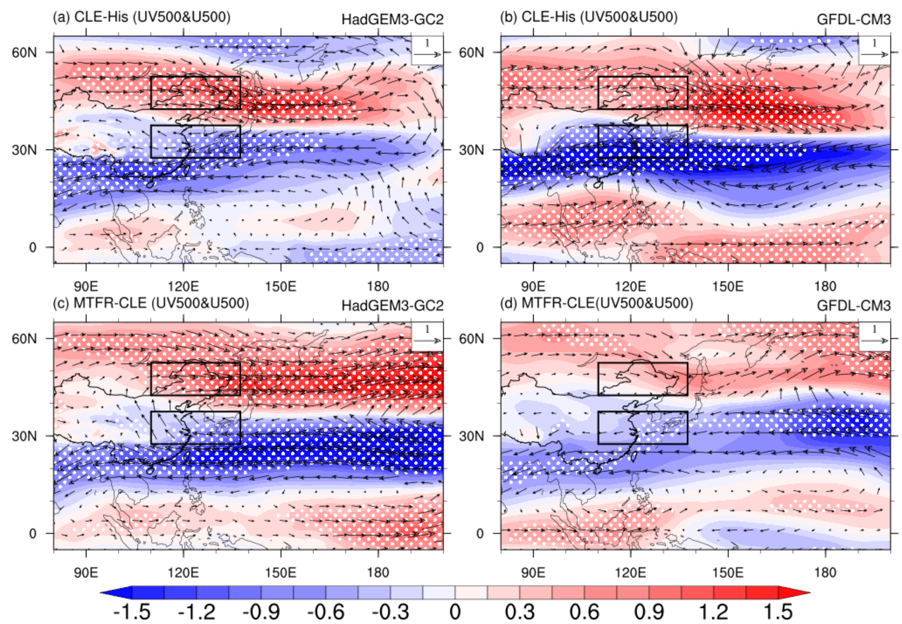

Fig.7 Same as Fig.6, but for the difference in 500hPa winds (vector, m s^{-1}) and 500hPa zonal component (shading, m s^{-1}).

https://doi.org/10.5194/acp-2020-957
Preprint. Discussion started: 12 October 2020

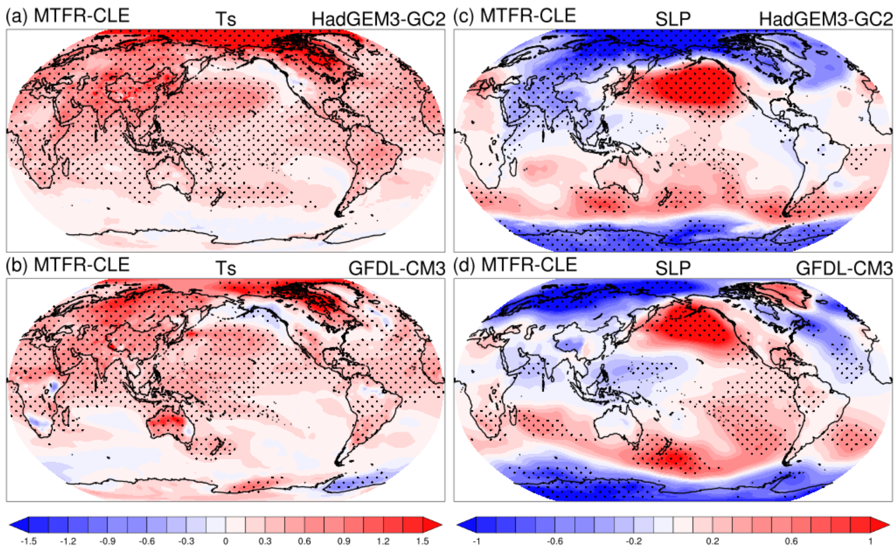

Fig.8 The difference of the climate mean surface temperature (left, K) and sea level pressure (right, hPa) between MTFR and CLE simulated by (a)-(b) HadGEM3-GC2 and (c)-(d) GFDL-CM3.

https://doi.org/10.5194/acp-2020-957
Preprint. Discussion started: 12 October 2020

Atmospheric Chemistry and Physics
Discussions

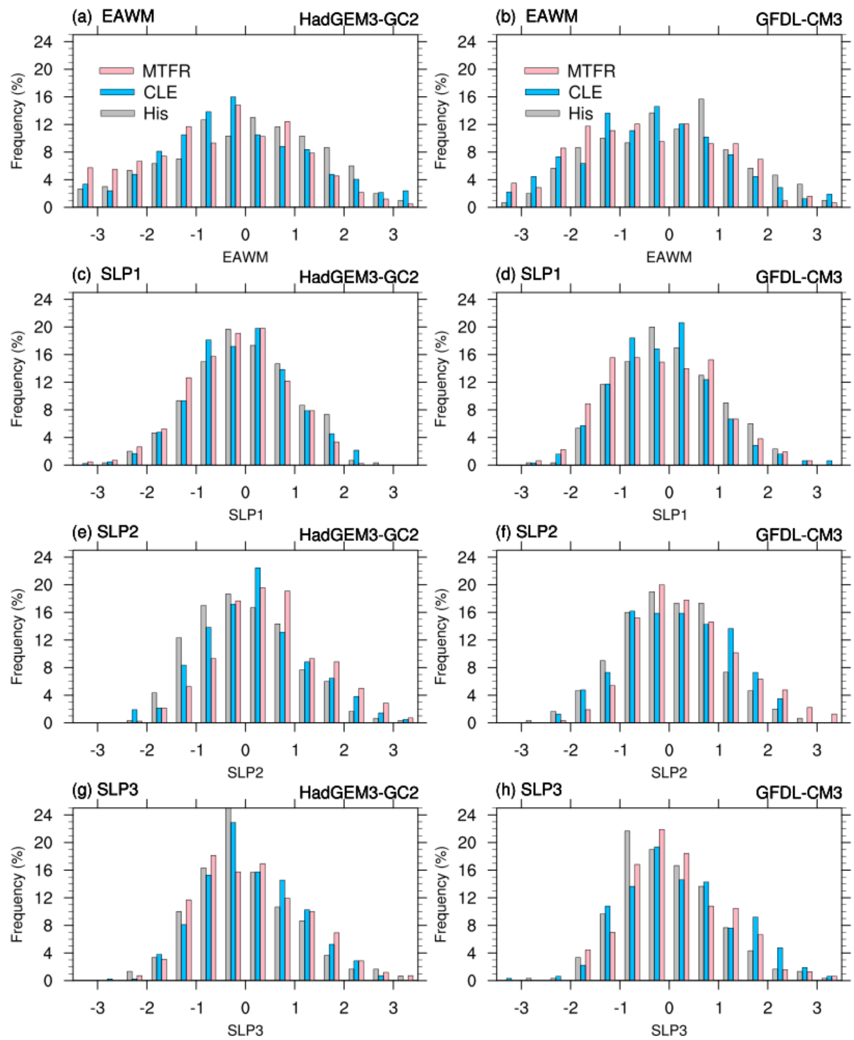

Fig.9 Same as Fig.4, but for histograms of the East Asian winter monsoon index and its components. SLP_1, SLP_2 and SLP_3 stand for the SLP averaged over Siberia, North Pacific and Maritime continent, respectively.

https://doi.org/10.5194/acp-2020-957
Preprint. Discussion started: 12 October 2020

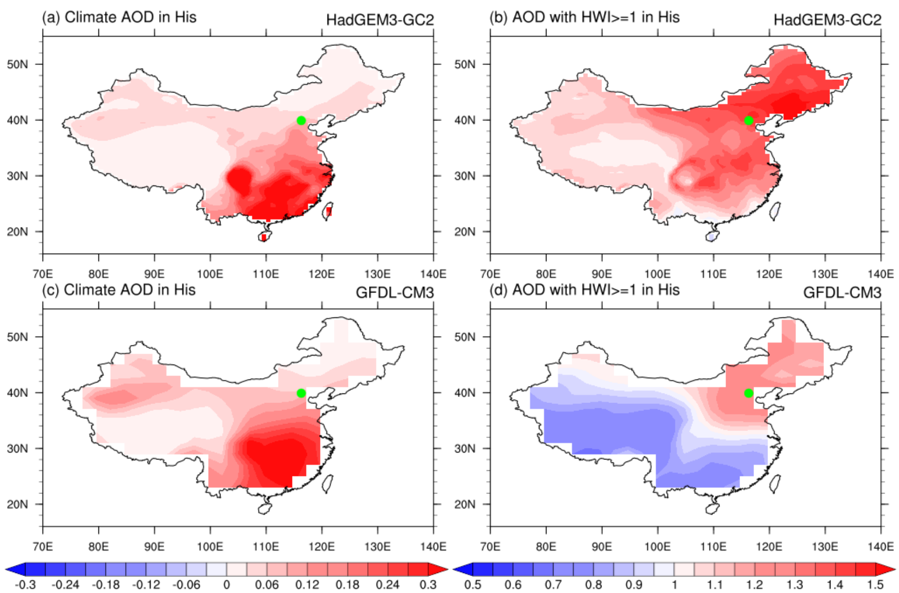

Fig.10 DJF mean (left) AOD at 550 nm in (a) HadGEM3-GC2 and (c) GFDL-CM3 averaged over 1980-2004. Right is same as left, but for the ratio of AOD (unit: %) averaged in the winter months with HWI≥1 relative to winter mean of 1980-2004. Blue and red shadings in (c)-(d) are lower and higher than the climate winter mean of His, respectively.

https://doi.org/10.5194/acp-2020-957
Preprint. Discussion started: 12 October 2020

Atmospheric Chemistry and Physics Discussions

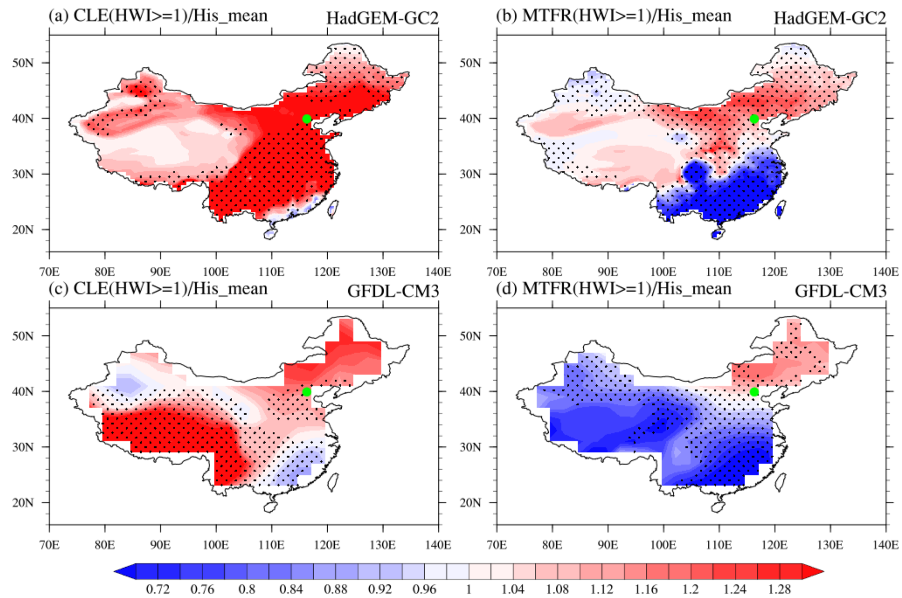

Fig 11. Same as Fig.10b and d, but for the results projected in CLE and MTFR. The baseline is the winter mean of 1980-2004.

https://doi.org/10.5194/acp-2020-957
Preprint. Discussion started: 12 October 2020

Atmospheric Chemistry and Physics Discussions

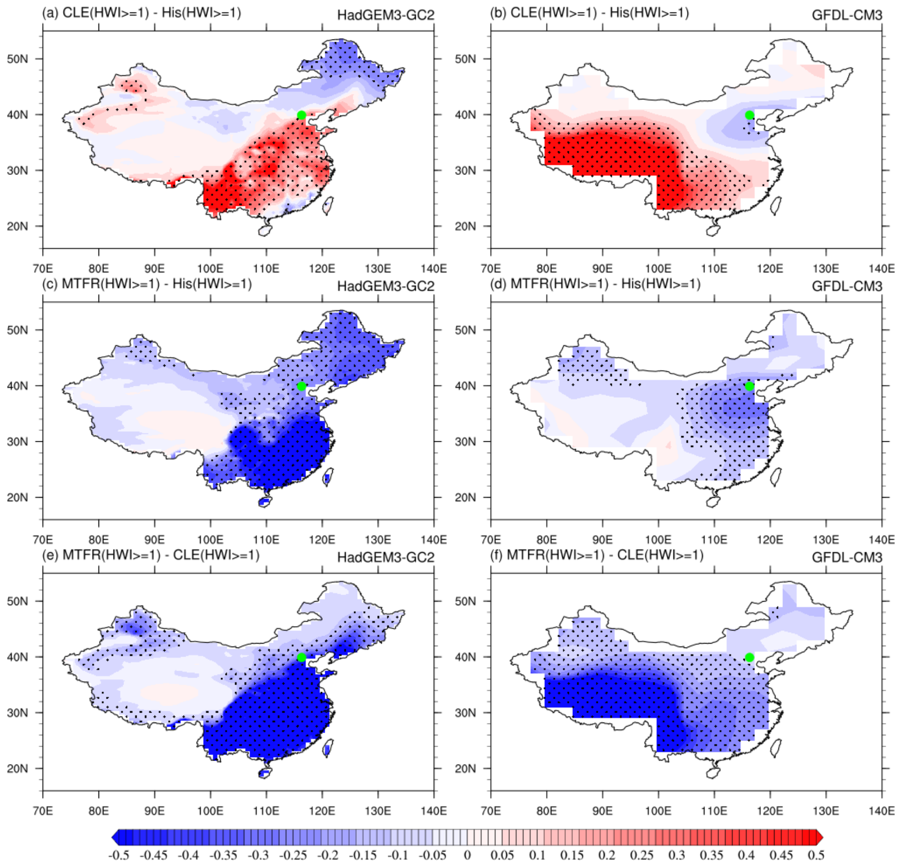

Fig. 12 Difference between the ratio of AOD when HWI≥1.0 to His winter mean in CLE and ratio of AOD when HWI≥1.0 to His winter mean in His in (a) HadGEM3-GC2 and (b) GFDL-CM3. (c)-(d) and (e)-(f) are same as (a) and (b), but for the difference between MTFR and His and the difference between MTFR and CLE, respectively. Blue and red shadings indicate projected AOD when HWI≥1.0 is lower and higher than the AOD when HWI≥1.0 in His, respectively.